JOURNAL OF SPACECRAFT AND ROCKETS
Vol. 48, No. 1, January–February 2011

# Substitution of Hot-Gas Lateral Jets by Cold-Gas Jets in Supersonic Flows

F. Sourgen,* T. Gauthier,† F. Leopold,‡ and B. Sauerwein§
*French–German Research Institute of Saint-Louis, 68301 Saint-Louis, France*
and
R. Meuer¶
*Rheinmetall Waffe Munition GmbH, 29345 Unterluess, Germany*

DOI: 10.2514/1.50543

**The supersonic flow around a rocket piloted by thrusters has been investigated. Steady Reynolds-averaged Navier–Stokes computations and pressure measurements in a wind tunnel, using pressure taps and pressure-sensitive paint, have been performed. For experimental investigations, real hot-gas thrusters have been replaced by cold-gas jets using a lower total pressure and a different gas. The uniqueness of this work involved calibrating those cold-gas thrusters in order to reproduce an aerodynamic interference very similar to the hot-gas jets case. This has been achieved by modifying the section ratio of the nozzles in order to control the wave celerity ratio between freestream and jet flows. A good agreement has been obtained between numerical simulations of hot-gas and cold-gas jets flows, as well as between computations and measurements of the pressure coefficient around the body in the wind tunnel. Thus, this method has provided a good approximation for the interaction between hot-gas jets and crossflow by using lower-pressure and lower-temperature jets.**

## Nomenclature

| | | |
|---|---|---|
| $\mathcal{C}$ | = | wave celerity similarity number |
| $C_f$ | = | friction coefficient |
| $C_p$ | = | pressure coefficient |
| $C_{p\ \mathrm{diff}}$ | = | differential pressure coefficient |
| $D$ | = | diameter of the body, m |
| $\mathcal{J}$ | = | momentum flux similarity number |
| $JR$ | = | momentum flux ratio |
| $\mathcal{M}$ | = | mass flux similarity number |
| $M_{\mathrm{th}}$ | = | thruster ejection Mach number |
| $M_\infty$ | = | freestream Mach number |
| NCR | = | nozzle celerity ratio |
| NJR | = | nozzle momentum flux ratio |
| NMR | = | nozzle mass flux ratio |
| NPR | = | nozzle pressure ratio |
| NrTR | = | nozzle temperature ratio |
| $\mathcal{P}$ | = | pressure similarity number |
| PR | = | total pressure ratio |
| $P_j$ | = | nozzle exit static pressure, Pa |
| $P_o$, $P_\infty$ | = | freestream static pressure, Pa |
| $P_t$ | = | total pressure, Pa |
| $P_{ti}$ | = | thruster stagnation pressure, Pa |
| $Re_D$ | = | diameter-based Reynolds number |
| $r_{\mathrm{th}}$ | = | specific thruster gas constant, $\mathrm{J \cdot kg^{-1} \cdot K^{-1}}$ |
| $r_\infty$ | = | specific freestream gas constant, $\mathrm{J \cdot kg^{-1} \cdot K^{-1}}$ |
| $\mathcal{T}$ | = | temperature similarity number |
| $T_j$ | = | nozzle exit static temperature, K |
| $T_t$ | = | total temperature, K |
| $T_{ti}$ | = | thruster stagnation temperature, K |
| $T_\infty$ | = | freestream static temperature, K |
| $U$ | = | velocity component along the $x$ axis, $\mathrm{m \cdot s^{-1}}$ |
| $U_o$, $U_\infty$ | = | freestream velocity component along the $x$ axis, $\mathrm{m \cdot s^{-1}}$ |
| $u_f$ | = | friction velocity component along the $x$ axis, $\mathrm{m \cdot s^{-1}}$ |
| $W$ | = | velocity component along the mean ejection direction, $\mathrm{m \cdot s^{-1}}$ |
| $W_j$ | = | nozzle exit velocity component along the mean ejection direction, $\mathrm{m \cdot s^{-1}}$ |
| $x$ | = | horizontal coordinate along the body axis, m |
| $y$ | = | horizontal coordinate perpendicular to the body axis, m |
| $y^+$ | = | dimensionless wall distance |
| $z$ | = | vertical coordinate, m |
| $\gamma_{\mathrm{th}}$ | = | thruster gas isentropic coefficient |
| $\gamma_\infty$ | = | freestream gas isentropic coefficient |
| $\nu$ | = | kinematic viscosity, $\mathrm{m^2 \cdot s^{-1}}$ |
| $\rho$ | = | density, $\mathrm{kg \cdot m^{-3}}$ |
| $\rho_j$ | = | nozzle exit density, $\mathrm{kg \cdot m^{-3}}$ |
| $\rho_\infty$ | = | freestream density, $\mathrm{kg \cdot m^{-3}}$ |
| $\tau_w$ | = | wall shear, Pa |

Received 28 April 2010; revision received 8 July 2010; accepted for publication 15 July 2010. Copyright © 2010 by the French–German Research Institute of Saint-Louis. Published by the American Institute of Aeronautics and Astronautics, Inc., with permission. Copies of this paper may be made for personal or internal use, on condition that the copier pay the $10.00 per-copy fee to the Copyright Clearance Center, Inc., 222 Rosewood Drive, Danvers, MA 01923; include the code 0022-4650/11 and $10.00 in correspondence with the CCC.

*Researcher, Aerodynamics and Wind Tunnels Department, 5 rue du Général Cassagnou, P.O. Box 70034; frederic.sourgen@isl.eu. Member AIAA.

†Engineer, Aerodynamics and Wind Tunnels Department, 5 rue du Général Cassagnou, P.O. Box 70034; thibaut.gauthier@isl.eu. Member AIAA.

‡Head of Aerodynamics and Wind Tunnels Department, 5 rue du Général Cassagnou, P.O. Box 70034; friedrich.leopold@isl.eu.

§Engineer, Aerodynamics and Shock Tubes Department, 5 rue du Général Cassagnou, P.O. Box 70034; berthold.sauerwein@isl.eu.

¶Research and Development Engineer, Fluid Dynamics Department, Heinrich Ehrhardt Strasse 2, P.O. Box 201403; rosemarie.meuer@rheinmetall.com.

## I. Introduction

GAS-EJECTION-BASED actuators have proved to be efficient to quickly change trajectories of missiles and rockets in various flight conditions [1,2]. However, ejection of a gas along the lateral direction strongly modifies the surface pressure distribution around the body, due to the interference with the surrounding flow. The 3-D structure of the interaction can also modify the pressure distribution on surrounding lift surfaces and introduce unsteadiness [3,4]. The duration of this kind of action is typically about a few milliseconds to a few seconds. Consequently, the interference between lateral jets and crossflow can have important consequences on in-flight behavior. For this reason, aerodynamic effects related to this kind of actuator have been accurately investigated in the last decades. Because of the considerable experimental [3,5,6] and numerical

work [7–12] accomplished on this subject, the nature of these effects and the structure of the interference between the lateral jet and crossflow are currently well known [13–21].

However, numerical tools still need to be calibrated to correctly predict this kind of flow as well as in-flight behavior. This means that experiments in the wind tunnel remain essential. The problem is that producing stable high pressure and temperature jets is technically difficult. Pyrotechnical devices have to be employed, which means that stability and accurate control of pressure and temperature conditions are not guaranteed. In addition, a blockage can occur in the wind tunnel due to high pressure and temperature gas ejection in the limited test section. This particularly limits the use of low-cost laboratory wind tunnels for this kind of study.

In addition to technical difficulties, it is not always possible to reproduce the real flight conditions in a blow down wind tunnel. A shock tube can be used instead, but the duration of the experiments is usually very short.

Indeed, ground testing for this kind of flow usually consists of using hot or cold-gas jets, calibrated to keep a few of the real parameters, such as total pressure ratio or momentum flux, to reproduce the mechanical thrust. Using these partly similar conditions, the aerodynamic interferences can be different between the real flow case and the case investigated in the experimental facility. Therefore, the distribution of the pressure coefficient around the body as well as the 3-D structure of the flow can be very different.

In this paper, a scaling method is described in order to obtain a better approximation of the real interference between hot-gas lateral jets and the surrounding supersonic flow, by using cold-gas and lower-pressure jets instead. Numerical simulations using the Reynolds-averaged Navier–Stokes equations approach have been used as a tool to validate the method. The capability of the method to reproduce the real pressure coefficient in the wind tunnel has been evaluated using pressure taps and pressure-sensitive-paint technique.

## II. Method

### A. Choice of Similarity Parameters

To properly scale experiments, similarity parameters have to be chosen. A general approach is suggested for the interaction between the lateral jet and the supersonic flow, whose main aspects are represented in Fig. 1 [1].

When investigating this kind of flow, the total pressure and momentum flux ratios are commonly used parameters, since they describe the mechanical thrust. They are defined by Eqs. (1) and (2):

$$\mathrm{PR} = \frac{P_t}{P_\infty} \tag{1}$$

$$JR = \frac{\rho W^2}{\rho_\infty U_\infty^2} \tag{2}$$

For now, two cases of interference between lateral jet and supersonic flow are under consideration. The Mach number of the freestream flow and the shape of the body in each case are assumed to be the same. However, the body diameter, the gases, the section ratios as well as the stagnation conditions for the thrusters and the freestream values of pressure and temperature can be different. The first case is called the *real* configuration and the second one will be the *similar* configuration. Then, taking into account the characteristics of each flow, several parameters can be built using Eqs. (3–8):

$$Re_D = \frac{U_\infty D}{\nu_\infty} \tag{3}$$

$$\mathrm{NPR} = \frac{P_j}{P_\infty} = \mathrm{PR} \cdot \left(1 + \frac{\gamma_{\mathrm{th}} - 1}{2} M_{\mathrm{th}}^2\right)^{\frac{-\gamma_{\mathrm{th}}}{\gamma_{\mathrm{th}}-1}} \tag{4}$$

$$\mathrm{NrTR} = \frac{r_{\mathrm{th}} T_j}{r_\infty T_\infty} = \frac{r_{\mathrm{th}} T_i}{r_\infty T_\infty (1 + \frac{\gamma_{\mathrm{th}}-1}{2} M_{\mathrm{th}}^2)} \tag{5}$$

$$\mathrm{NJR} = \frac{\rho_j (W_j)^2}{\rho_\infty (U_\infty)^2} = \mathrm{NPR} \frac{\gamma_{\mathrm{th}} M_{\mathrm{th}}^2}{\gamma_\infty M_\infty^2} \tag{6}$$

$$\mathrm{NMR} = \frac{\rho_j W_j}{\rho_\infty U_\infty} = \frac{\mathrm{NPR}}{\sqrt{\mathrm{NrTR}}} \sqrt{\frac{\gamma_{\mathrm{th}} M_{\mathrm{th}}^2}{\gamma_\infty M_\infty^2}} \tag{7}$$

$$\mathrm{NCR} = \frac{\sqrt{\gamma_{\mathrm{th}} r_{\mathrm{th}} T_j}}{\sqrt{\gamma_\infty r_\infty T_\infty}} = \sqrt{\frac{\gamma_{\mathrm{th}}}{\gamma_\infty}} \mathrm{NrTR} \tag{8}$$

The choice of the parameters defined by Eqs. (4–8) is based on several structural considerations. As hot-gas and cold-gas thrusters can have different shapes, the commonly used total pressure variable is replaced by the nozzle exit static pressure ratio [Eq. (4)]. This is particularly important for barrel shock and Mach disk structures, shown in Fig. 1. Note that this value remains theoretical. Indeed, due to the interaction with the crossflow, the pressure value at the nozzle exit is not a constant. However, it is used to account for the section ratio of the nozzles and the fact that the thrusters gases can be different. The theoretical nozzle exit static temperature ratio is also defined, taking into account the specific gas constant [Eq. (5)].

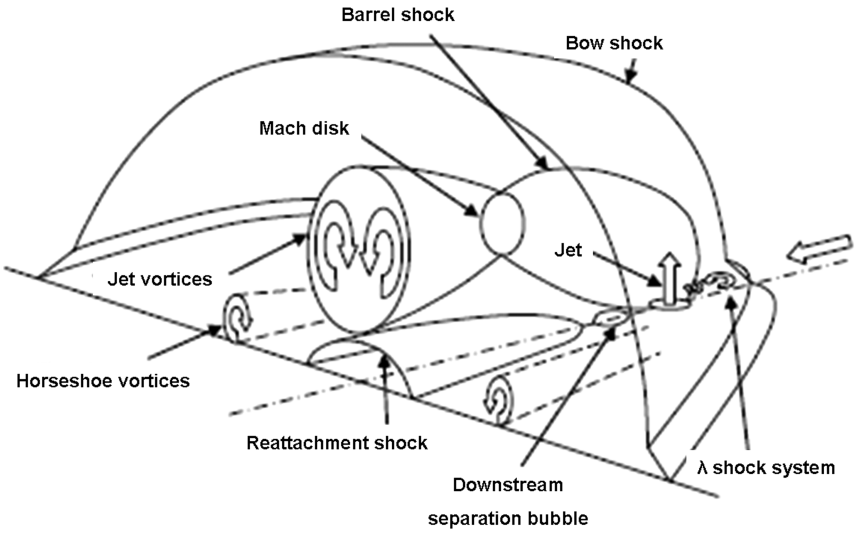


**Fig. 1 Structure of the aerodynamics interference between lateral jet and supersonic flow, reprinted from Champigny and Lacau [1].**

As mentioned above, the momentum flux describes the mechanical effect of thrusters [Eq. (6)]. In addition, the mass flux of the lateral jets compared to the freestream value is particularly important for the jet-layer development [Eq. (7)].

Finally, the most important parameter might be the relative values of wave celerity, in order to correctly account for the formation of oblique shock waves at the nozzle exit as well as for the development of the low-pressure region downstream [Eq. (8)].

These parameters are named similarity parameters. In practice, the ratios of these parameters between the two configurations are used. They are named similarity numbers and are defined by Eqs. (9–13):

$$\mathcal{P} = \frac{\mathrm{NPR}^{\mathrm{similar}}}{\mathrm{NPR}^{\mathrm{real}}} \tag{9}$$

$$\mathcal{T} = \frac{\mathrm{NrTR}^{\mathrm{similar}}}{\mathrm{NrTR}^{\mathrm{real}}} \tag{10}$$

$$\mathcal{J} = \frac{\mathrm{NJR}^{\mathrm{similar}}}{\mathrm{NJR}^{\mathrm{real}}} \tag{11}$$

$$\mathcal{M} = \frac{\mathrm{NMR}^{\mathrm{similar}}}{\mathrm{NMR}^{\mathrm{real}}} \tag{12}$$

$$\mathcal{C} = \frac{\mathrm{NCR}^{\mathrm{similar}}}{\mathrm{NCR}^{\mathrm{real}}} \tag{13}$$

Note that these numbers are not independent. They are related by the two following Eqs. (14) and (15):

$$\mathcal{C} = \sqrt{\frac{\gamma_{\mathrm{th}}^{\mathrm{similar}}}{\gamma_{\infty}^{\mathrm{similar}}} \frac{\gamma_{\infty}^{\mathrm{real}}}{\gamma_{\mathrm{th}}^{\mathrm{real}}}} \sqrt{\mathcal{T}} \tag{14}$$

$$\mathcal{M} = \sqrt{\frac{\mathcal{J}.\mathcal{P}}{\mathcal{T}}} \tag{15}$$

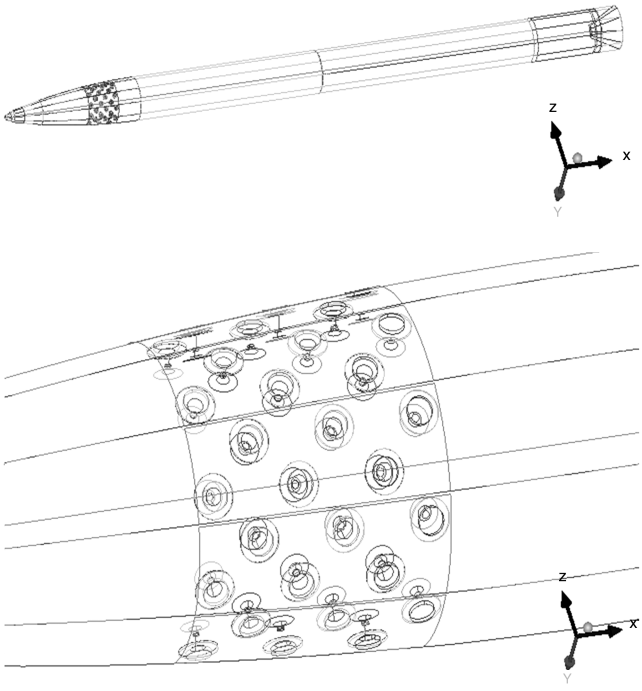


**Fig. 2 Geometry of a real rocket piloted by multiple thrusters.**

**Table 1 Characteristics of real flow and similar flow**

| Air, crossflow Mach 2 | Real hot-gas configuration | Similar cold-gas configuration |
|---|---|---|
| $P_{\infty}$, bar | 0.8 | 0.575 |
| $T_{\infty}$, K | 288 | 167 |
| Scale | 1 | 0.608 |
| Thruster gas | MRT | He |
| $M_{\mathrm{th}}$ | 2.92 | 2.25 |
| $P_{ti}$, bar | 750 | 163 |
| $T_{ti}$, K | 2700 | 288 |

A way to obtain similar aerodynamic interferences in the two configurations could be to keep these similarity numbers equal to one. This could be achieved by a judicious choice of gases, section ratios of thrusters, and stagnation conditions.

### B. Real Flow and Similar Flow Under Consideration

The supersonic flow at Mach number 2 around a rocket equipped with several simultaneously active thrusters is under consideration. The real geometry of the rocket is shown in Fig. 2. The nozzle's shape is shown in Fig. 3a. Real flight conditions and characteristics of the thrusters are summarized in Table 1. The gas used for the thrusters, called MRT (mikroreaktions triebwerk) gas, results from the combustion of a pyrotechnical composition. Only its isentropic coefficient and specific gas constant are known:

$$\gamma_{\mathrm{th}}^{\mathrm{real}} = 1.224$$

$$r_{\mathrm{th}}^{\mathrm{real}} = 331\ \mathrm{J \cdot kg^{-1} \cdot K^{-1}}$$

To reproduce the aerodynamic interference related to these hot-gas lateral jets, a cold-gas configuration has to be built while keeping the above mentioned similarity numbers as close to 1 as possible.

However, some additional constraints have to be taken into account. First, for the experiments in the wind tunnel, the freestream values of static pressure and temperature in the test section corresponding to Mach number 2 are imposed; their corresponding values are 0.575 bar and 167 K, respectively. The gas in the wind tunnel is air (rather than nitrogen, often used in shock tubes, for instance). Second, the cold gas used for thrusters will be stocked in industrial bottles, in which the temperature is typically 288 K. To simplify experiments this value will also be the stagnation temperature for cold-gas thrusters. At last, again to simplify wind-tunnel testing, the cold gas for thrusters is chosen to be helium, often used to simulate hot-gas jets, because of its low molar mass.

Under these additional constraints, it is no longer possible to keep each similarity number equal to one. Thus, the priority is given to the numbers corresponding to pressure $\mathcal{P}$, mass $\mathcal{M}$, and wave celerity $\mathcal{C}$. These three numbers correspond to three dependent equations to be solved to obtain the stagnation pressure and the ejection Mach number for cold-gas thrusters. In this way, the values 163 bar for the stagnation pressure and 2.25 for the Mach number have been found.

Once these values have been obtained, the accurate design of nozzles has to be chosen. Rather than making a simple biconical shape, the method of characteristics has been used to compute a cut Laval nozzle. In this way, the Mach number nominal value for cold-gas thrusters is obtained at the same ejection angle as real thrusters. The cold-gas nozzle defined in this manner is shown in Fig. 3b.

The other similarity numbers related to momentum flux $\mathcal{J}$ and exit temperature $\mathcal{T}$ are then determined. The Reynolds numbers ratio can easily be controlled by the caliber of the body in the cold-gas configuration. To have the same Reynolds number for the two configurations, the body in the similar configuration is scaled by a factor of 0.608 compared to the real case. The other similarity numbers have the following values: $\mathcal{P} = 1.00, \mathcal{C} = 1.07, \mathcal{M} = 1.00$, $\mathcal{J} = 0.82$, and $\mathcal{T} = 0.84$. The characteristics of the similar configuration obtained in this manner are summarized in Table 1. It

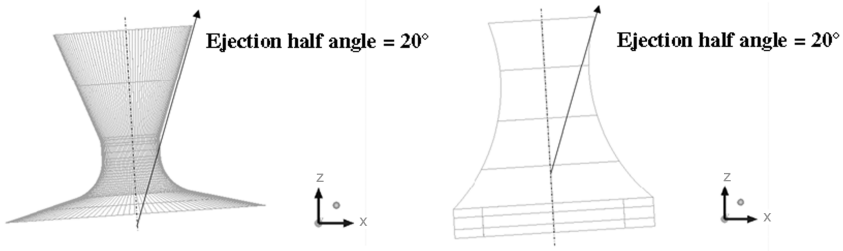


a) b)

**Fig. 3 Illustrations of a) real thruster and b) scaled thruster computed using the method of characteristics.**

can be observed that this configuration uses much lower-pressure and lower-temperature gas for lateral jets than does the real case.

## III. Numerical Simulations

### A. Numerical Method and Configurations Under Study

Numerical simulations have been used to validate the theoretical approach as well as to scale the model of the rocket for the wind-tunnel experiments. The steady Reynolds-averaged Navier–Stokes (RANS) method has been chosen, using CFX (ANSYS, Ltd.) [22]. The turbulence model used is the shear stress transport (SST) two-equation eddy-viscosity model from Menter [23]. Simulations have consisted of ideal gas mixture computations between two species: the gas chosen for thrusters, depending on the configuration, and air gas. Three configurations have been under study: 1) real hot-gas jets flow (air and MRT gas mixture), 2) similar cold-gas jets flow (air and helium gas mixture), and 3) wind-tunnel cold-gas jets flow (air and helium gas mixture in the test section).

The particular computational domain for the wind-tunnel configuration is shown in Fig. 4. It consists of half of a body fixed to the bottom wall of the test section. The computational domain for the real flow and the similar flow is shown in Fig. 5. For each configuration, the simultaneous action of three aligned thrusters has been investigated. The asymmetry of the geometry due to the existence of three other inactive thrusters is taken into account in the case of the complete 3-D simulations, as shown in Fig. 4. Note that the inlets of inactive thrusters have been replaced by a wall boundary condition.

The whole real rocket is several meters long and decimeters in width. The limited test section of the wind tunnel does not allow to keep the scale of 0.608 defined for the cold-gases configuration. A scaling factor of 0.25 has been chosen instead. Furthermore, the Reynolds number in wind tunnel is not equal to the real and similar flow cases, but it remains in the same region. Considering the environment in a wind tunnel, especially the influence of walls and arising turbulence, this is sufficient.

To save computational resources, only the front part of the complete rocket is modeled in each configuration, as shown in Figs. 4 and 5. The downstream region extends out to 2.5 body diameters after the last thruster.

### B. Boundary Conditions, Grids, and Numerical Accuracy

Two kinds of numerical simulations have been performed. Preliminary RANS computations of both configurations, using coarse tetrahedral meshes, have allowed to obtain a first validation of the theoretical approach as well as to build a well conditioned initial flow for computations on the finer meshes. The computational domains have consisted of complete 3-D domains, taking into account the nozzle and the walls of the test section in the case of the wind-tunnel configuration.

RANS computations of the real and similar configurations with a finer discretization using multiblocked structured meshes have produced more accurate results than with measurements. However, the high computational cost has prevented performing complete 3-D simulations. A half-3-D domain has been used instead. In this case, a free-slip wall boundary condition has been used for the symmetry plane of the rocket. The boundary conditions for each configuration are shown in Figs. 6–8.

For fine RANS computations, the mesh is first built for the real case. It consists of 2.1 million hexahedral elements discretizing the half-3-D domain. Figure 9 shows several parts of this mesh. It can be observed that it has been highly refined at the rocket nose, since the bow shock formed at this location will interact with the gas ejection

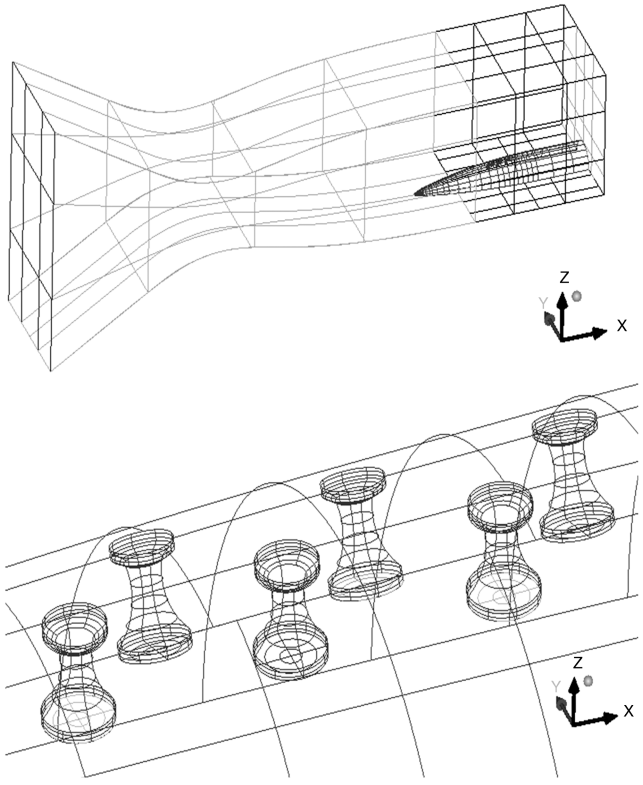


**Fig. 4 Wind-tunnel configuration and scaled thrusters.**

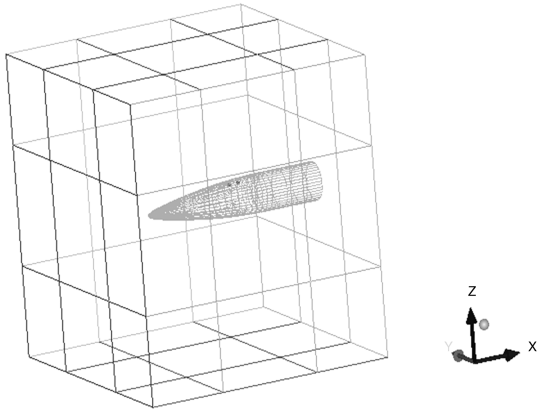


**Fig. 5 Real flow and similar flow computations.**

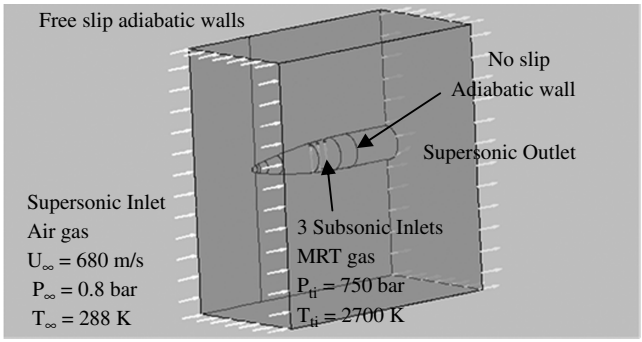


**Fig. 6 Boundary conditions for real flow computations.**

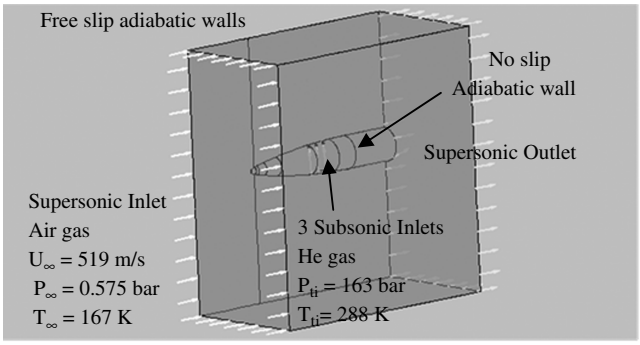


**Fig. 7 Boundary conditions for similar flow computations.**

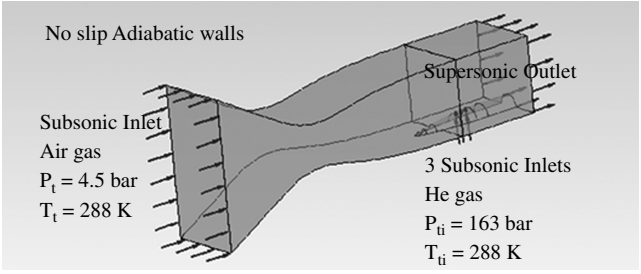


**Fig. 8 Boundary conditions for wind-tunnel flow computations.**

downstream. For the same reason, the upstream shape of the rocket has been refined.

All along the shape of the body, the first edge wall distance is about 1 $\mu$m, providing for a dimensionless first distance $y^+$ of approximately unity. A coarse-to-fine mesh resolution study was performed in precedent investigations and a grid convergence was obtained [24,25]. However, in order to save computational cost due to mesh size, the mesh expansion factor was always chosen equal to 1.4. This value is slightly larger than ratios currently used to ensure a properly resolved boundary layer (about 1.3 or less) and should be validated by experimental data. These are usually important considerations for near-wall laws and for a correct use of the SST turbulence model [22]. They are absolutely essential in the particular case of the interaction between lateral jet and supersonic flow [18,19].

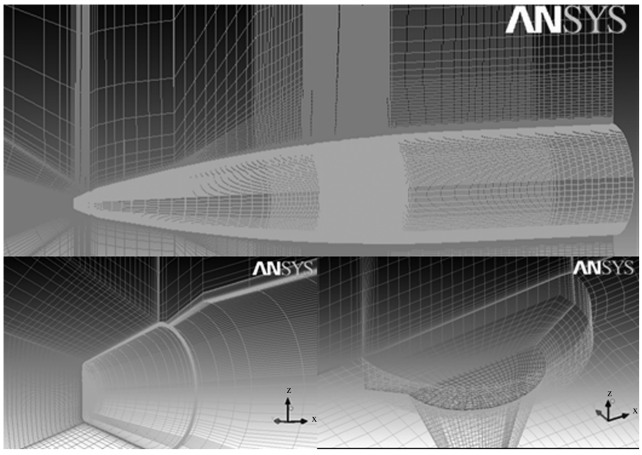


**Fig. 9 Mesh for fine RANS computations (real flow).**

Once the mesh has been built for the real flow, it is multiplied by the scale factor in order to obtain the mesh for the external flow in the similar configuration; the dimensionless distance $y+$ should remain near unity. This can be justified by considering that the friction coefficient should approximately have the same value in the two cases, since the similarity numbers, especially the Reynolds number, have the same values. Therefore, the first edge wall distances should be in proportion of the scale factor. This is illustrated by Eqs. (16–18):

$$u_f = \sqrt{\tau_w/\rho} \tag{16}$$

$$C_f = \frac{\tau_w}{\frac{1}{2}\rho_\infty U_\infty^2} = f(Re_D, \text{NPR}, \text{NMR}, \text{NCR}, \text{NJR}, \text{NrTR}) \tag{17}$$

$$y^+ = \frac{yu_f}{\nu} = \frac{yU_\infty}{\nu}\sqrt{\frac{C_f}{2}} = \frac{y}{D}F(Re_D, \text{NPR}, \text{NMR}, \text{NCR}, \text{NJR}, \text{NrTR}) \tag{18}$$

Indeed, the mesh inside the thrusters should have been modified, since they have a different shape, but the same degree of refinement has been kept.

The numerical simulations have been performed using a high-discretization scheme for each transport equation, giving a second-order solution. For each configuration, a physical time scale of 10 $\mu$s has been used and the computation has been stopped when the maximum residuals for all the transport equations have been lower than 0.002 (convergence criterion).

### C. Numerical Results

Quick computations using coarse tetrahedral meshes were used to validate the scaling of the wind-tunnel configuration and the location chosen for the body, as shown in Fig. 10. It can be observed in the

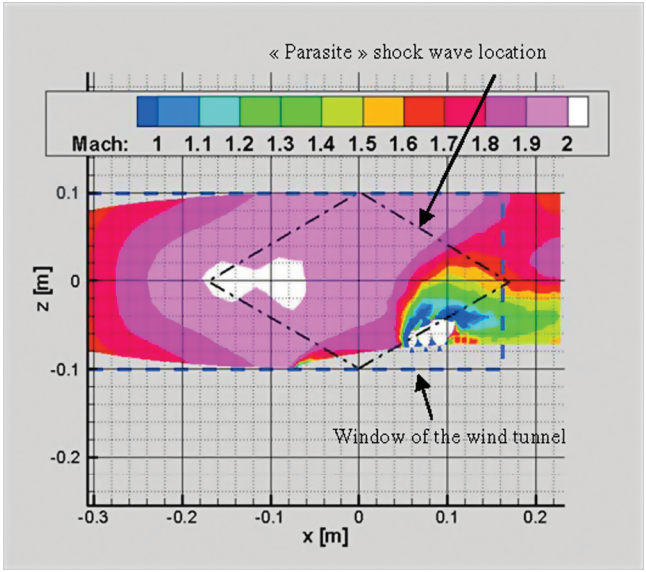


**Fig. 10 Mach number in the symmetry plane for RANS computation on the coarse grid of the wind-tunnel flow.**

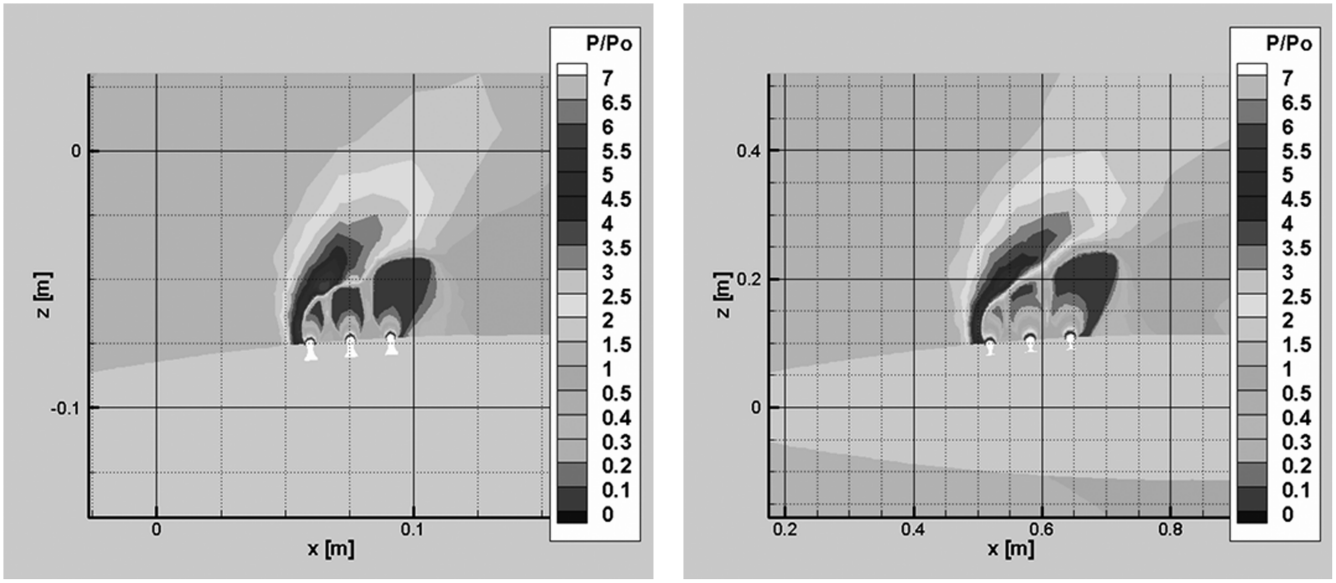


**a) Real flow** **b) Wind tunnel flow**

**Fig. 11 Scaled pressure in the symmetry plane for RANS computations on the coarse grid.**

Mach number distribution in the symmetry plane that no chocking occurs in the test section, in spite of the body and gas ejection. It can also be observed that the unwanted shock wave, denoted as parasite shock, formed at the junction between the nozzle and the test section does not interfere with the lateral jet and crossflow interaction. This is of prime importance for future pressure measurements along the body. It has been necessary to locate the body partly inside the nozzle of the test section but it can be seen that the upstream Mach number remains almost equal to 2.

The comparison of the real flow and wind-tunnel flow results allow the testing of the method. The pressure field in the symmetry plane of each configuration is pictured in Fig. 11. The surface pressure distribution is shown in Fig. 12. Note that some important physical aspects, such as boundary-layer separation, are not taken into account by such computations. However, a good agreement is found at this time between real flow and wind-tunnel flow for the low-pressure downstream region.

In addition, the influence of the walls in the wind tunnel can be estimated in Fig. 12b, which is crucial information for future instrumentation. Inside a 120° angular sector on both sides of the symmetry plane, the surface pressure distributions are similar for the two cases.

More accurate numerical results have been obtained using hexahedral meshes for real flow and similar flow. The pressure coefficient is shown in Fig. 13. The boundary-layer separation can be observed and the two simulations are in good agreement. Moreover, the friction coefficient shown in Fig. 14 has similar values in the two configurations. This result validates a posteriori the manner in which the mesh for the similar configuration has been deduced from the real configuration.

The horizontal velocity component, scaled by the freestream value, is shown in Fig. 15. A good agreement can again be observed for the boundary-layer separation and the bow shock formed at the front of the first jet, as well as for the rear part of the flow behind the third jet. However, in the interjet region, the velocity gradients are higher in the hot-gas jet's flow. This is most likely due to the much higher exit velocity and temperature than in the cold-gas jet configuration.

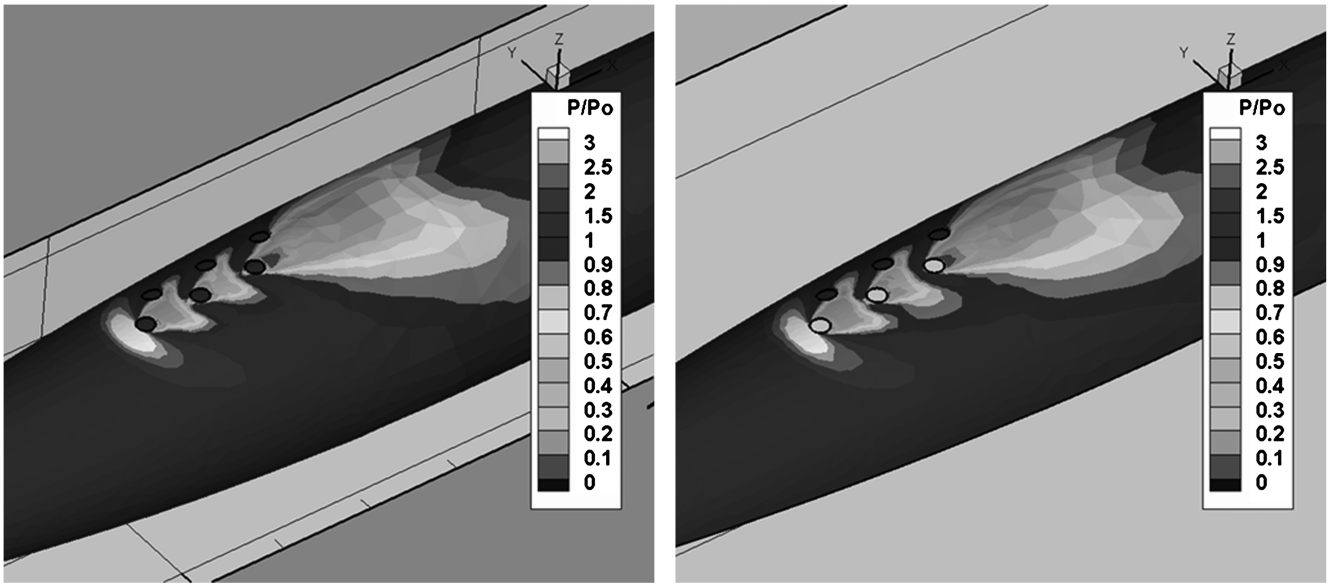


**a) Real flow** **b) Wind tunnel flow**

**Fig. 12 Surface scaled pressure for RANS computations on the coarse grid.**

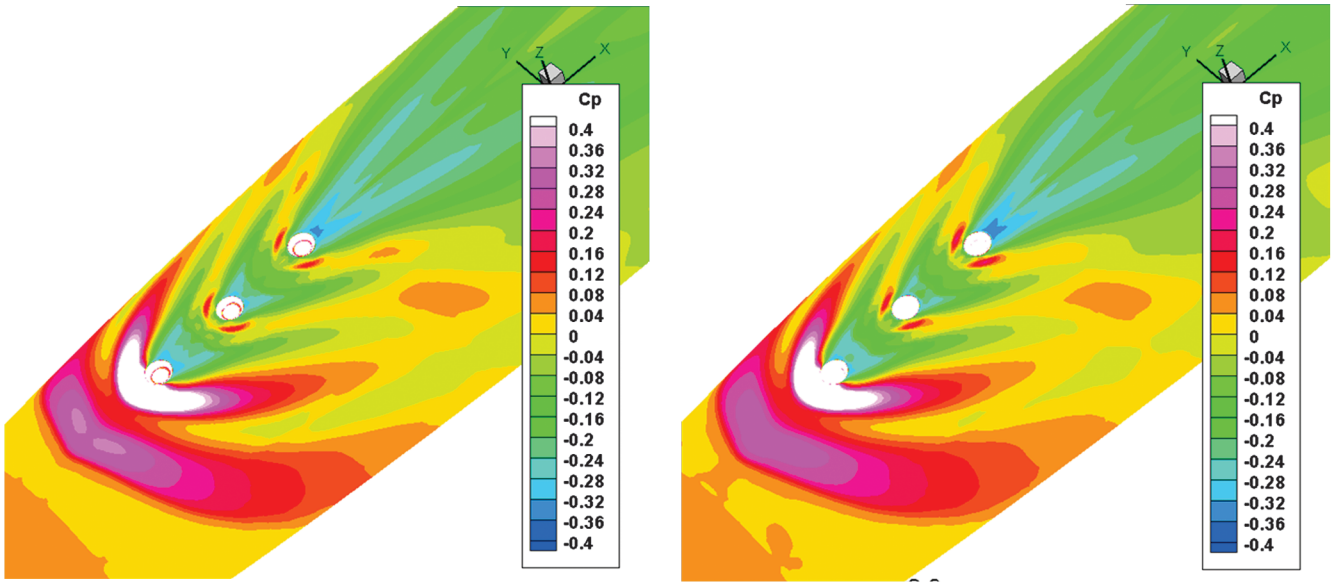


a) Real flow b) Similar flow

**Fig. 13 Pressure coefficient for RANS computations on the fine grid.**

Indeed, streamlines shown in Fig. 16 show that the horseshoe vortices and the downstream separation bubble in the two configurations are close in structure and dimensions.

## IV. Comparison with Measurements

### A. Experimental Facility and Instrumentation

Experiments have been performed in the blowdown wind tunnel of the French–German Research Institute of Saint-Louis. The test section is limited to a height and width of 200 mm. The test body is fixed at the bottom wall of the test section as shown in Fig. 17. The body has been positioned in order to avoid interference with the parasite shock wave formed at the junction between the test section and the nozzle used for Mach number 2.

The shape of the front part of the real rocket has been scaled by a factor of 0.25 and the body can be equipped with one to six thrusters. The inlets of inactive thrusters are simply blocked by a wall. In the configuration under study, the three thrusters in the symmetry plane have consisted in three cut Laval nozzles designed using an electroerosion process. The thrusters were fed by a pressure chamber located underneath the test section.

The chamber was supplied with helium gas at pressure and temperature nominal values by standard industrial bottles. A high speed opening and closing gate allowed saving helium gas during experiments and the experiment duration was typically about 400 ms. In this manner, several experiments could be performed before the pressure decreased in the helium bottles. The default pressure value in industrial bottles was 200 bars; the refilling of working bottles could be achieved using a pump.

Pressure and temperature in the chamber were controlled during experiments using high rate acquisition sensors. A 3% accuracy around the nominal value was obtained for the pressure, while the temperature was very stable.

The body in the test section was instrumented by pressure taps shown in Figs. 18 and 19. Kulite sensors were used. Although their sensible surface was 2.4 mm wide, the apparent diameter was limited to 0.6 mm, which is a value consistent with the assumed surface pressure gradients obtained in numerical simulations. The diameter reduction was obtained using the conical shape of the drill used, as shown in Fig. 18.

The pressure taps were distributed regularly in the symmetry plane, every 10 mm, from the assumed boundary-layer separation

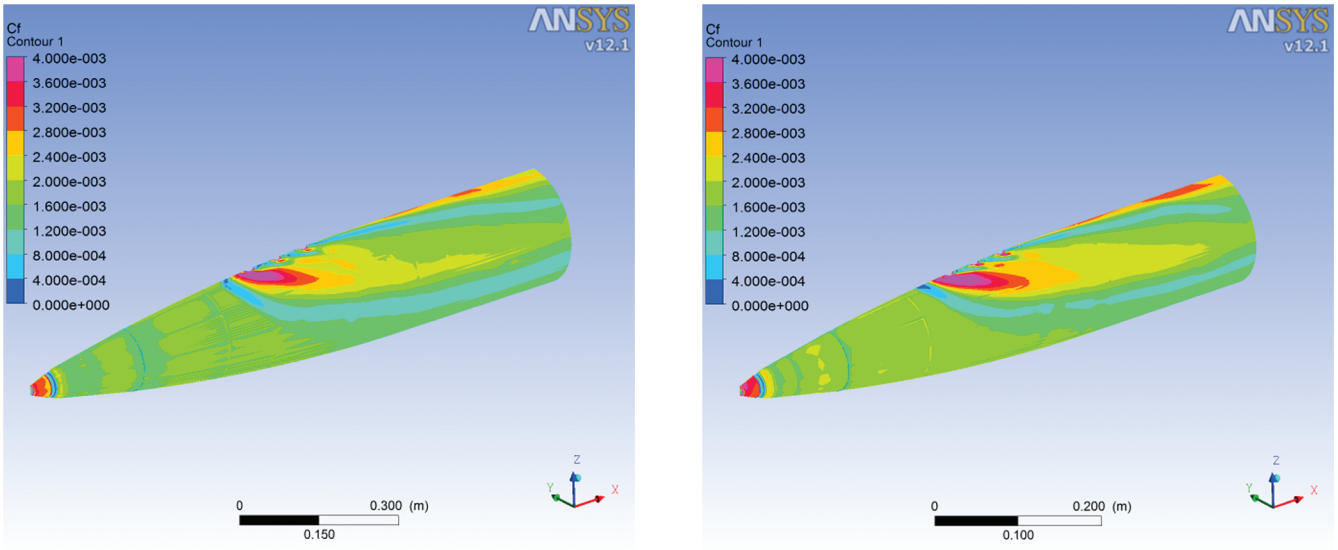


a) Real flow b) Similar flow

**Fig. 14 Friction coefficient for RANS computations on the fine grid.**

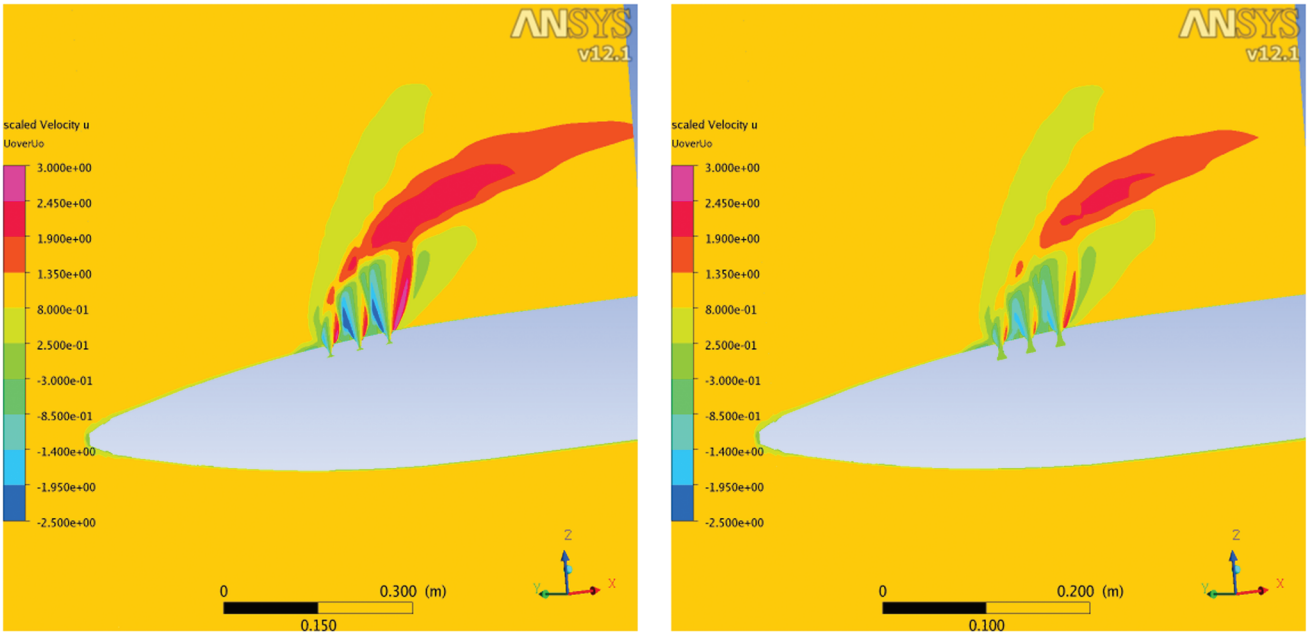


**a) Real flow** **b) Similar flow**

**Fig. 15 Scaled horizontal velocity component for RANS computations on the fine grid.**

region to the rear part of the body. Several angular repartitions have been added at ±18, ±36, and ±54°, as shown in Fig. 19. Beyond 60°, numerical simulation of the flow in the wind-tunnel configuration has predicted that the walls influenced the surface pressure noticeably. Finally, about 100 pressure measurement locations around the body have been available.

Pressure values have been measured using a high acquisition rate (20 kHz) during 250 ms, so that five thousand samples have been used to determine the pressure mean value and squared value. The statistical error [26] is estimated to 1% for the mean value and 2% for the squared value. Since the flow under investigation is very unsteady, the squared value was equal to about 30% of the mean value for most of the pressure taps.

### B. Pressure-Sensitive-Paint Measurements and Comparison to Computations

Because of considerable progress over the last decade in cameras, illumination sources, and paint formulation, the pressure-sensitive-paint (PSP) technique has been successfully applied to many complex flows in order to obtain a global and accurate surface pressure measurement [27–29]. This technique was used in addition to pressure sensors to measure the pressure coefficient around the body. The experimental setup is shown in Fig. 20.

Luminophore molecules in the base coat were applied to the body using a professional spray gun. The illumination light was supplied by a continuous light-emitting diode (25 W) at 405 nm. Luminescent intensity, which changes with near-surface pressure according to the

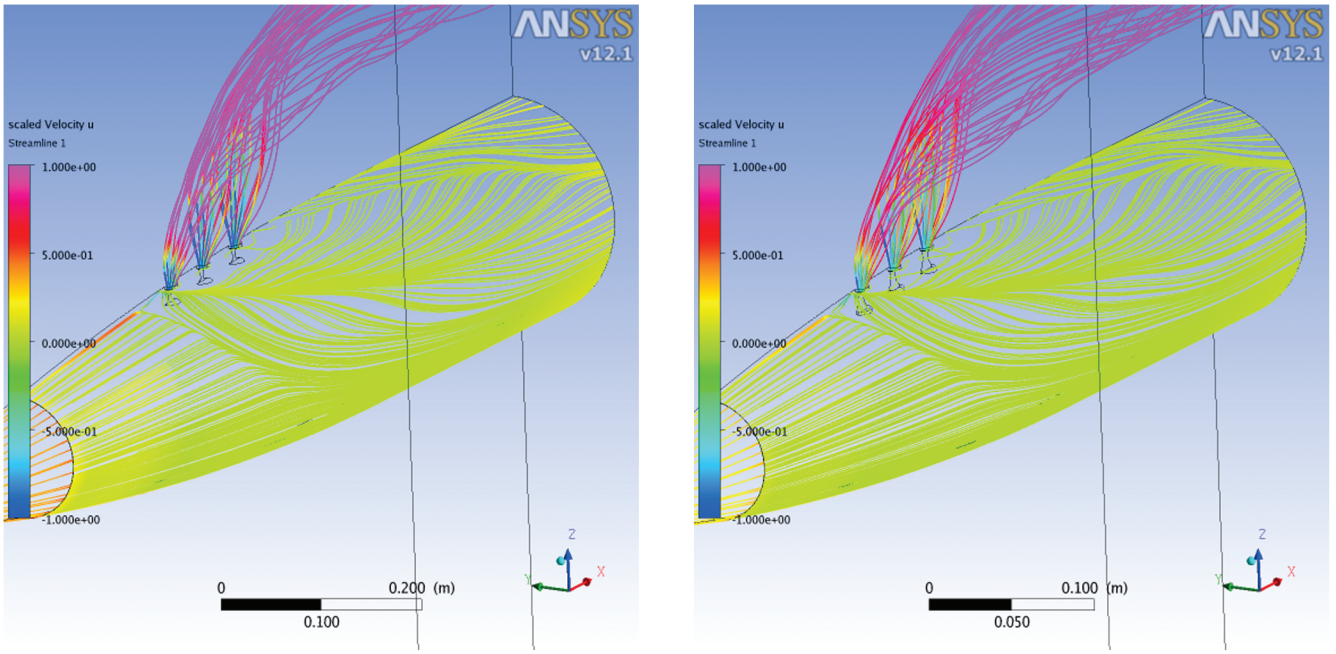


**a) Real flow** **b) Similar flow**

**Fig. 16 Streamlines for RANS computations on the fine grid.**

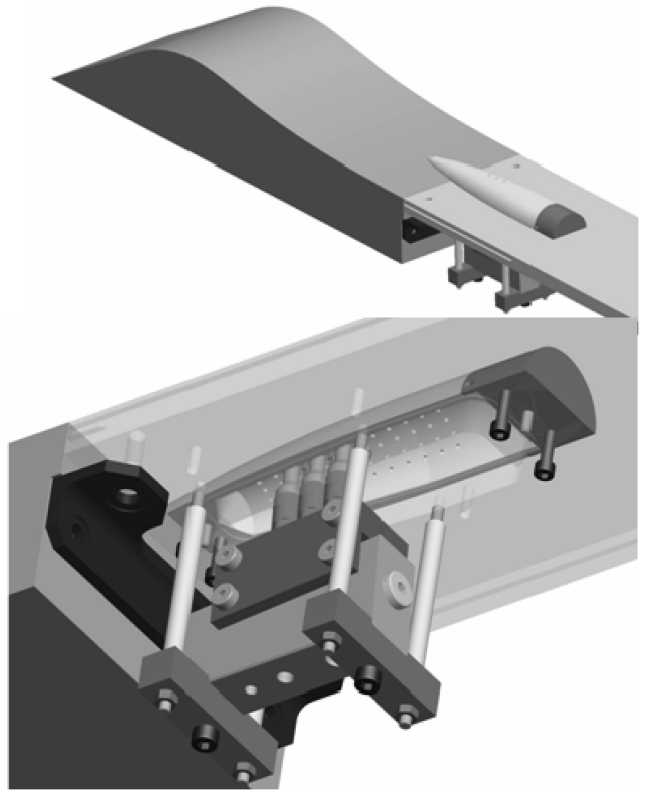

Fig. 17 Body in the test section.

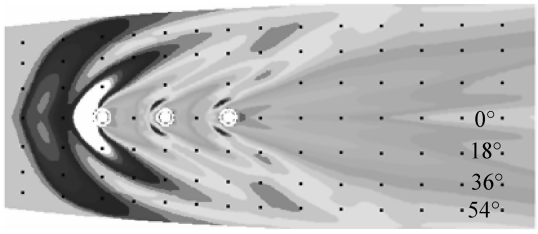


Fig. 19 Pressure-tap locations and diameters relatively to assumed surface pressure (RANS computation).

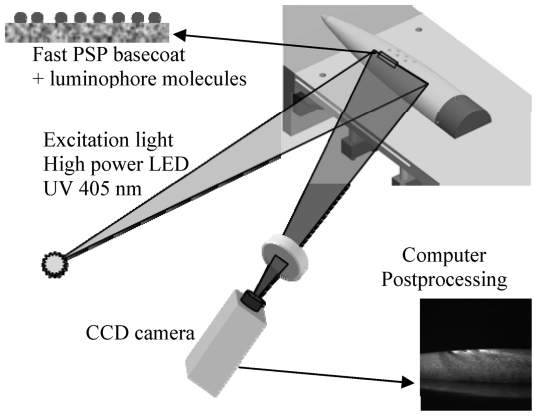


Fig. 20 Pressure-sensitive-paint experimental setup.

Stern–Volmer relation, was collected using a $1024 \times 1024$ pixel complementary metal oxide semiconductor camera. A filter centered at 650 nm was used to eliminate parasite light. The recording time was 20 ms, which is consistent with luminescent lifetime of the paint (1 ms).

A calibration and posttreatment method, developed at the French–German Research Institute of Saint-Louis [30], allowed for calibration of the paint, to reduce uncertainties and to map planar data onto the 3-D body surface.

At reference conditions, the wind-tunnel was turned on but the jets were turned off. In this manner, the differential pressure coefficient could be accurately measured. The use of this quantity, rather than the absolute pressure coefficient, allows for a partial filtering of the influence of the wind-tunnel environment.

In Fig. 21 the measured differential pressure coefficient can be compared to numerical simulation of the cold-gas jets configuration.

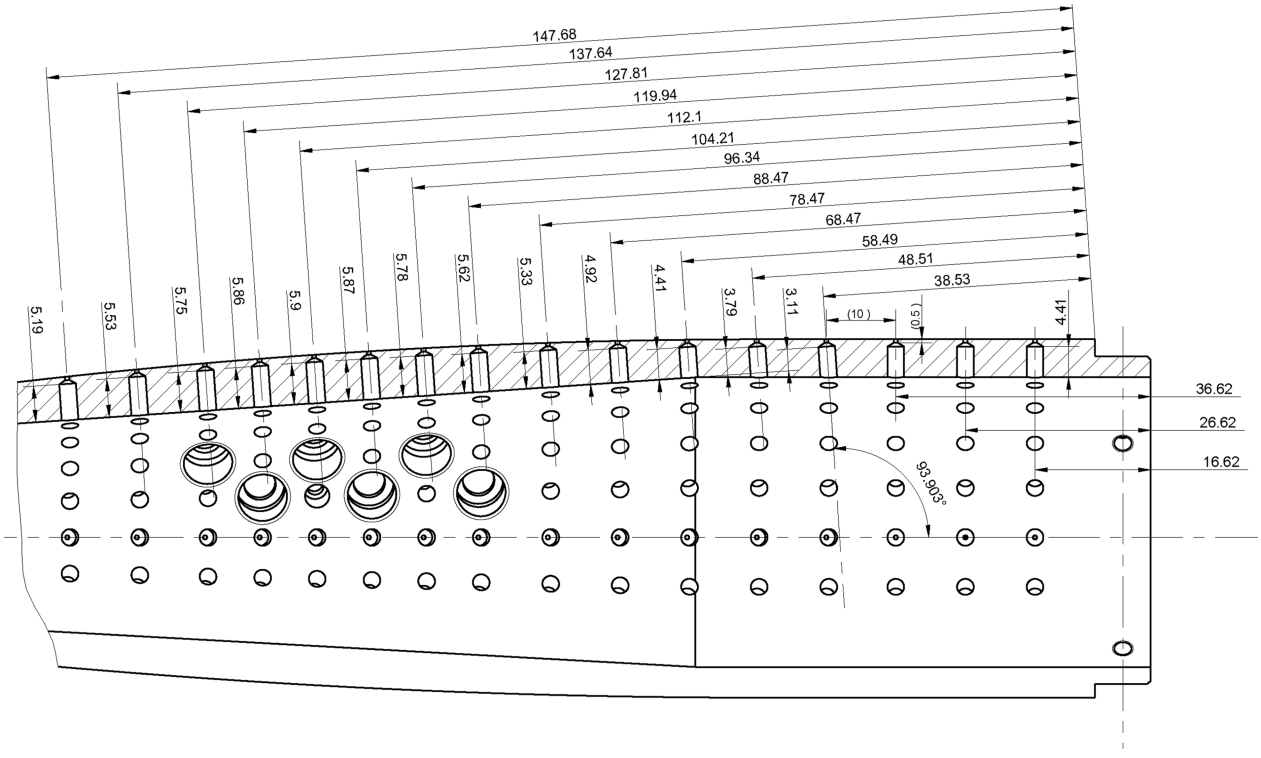


Fig. 18 Pressure-tap locations and shape.

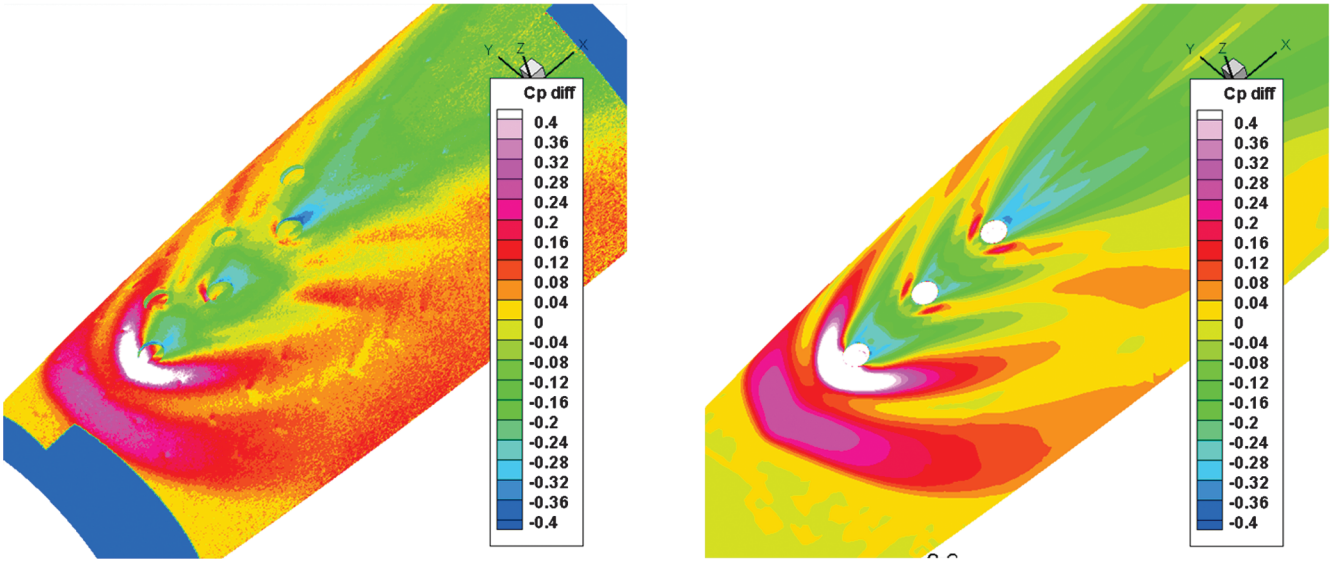


a) PSP measurement in wind tunnel b) Computation of the similar flow

Fig. 21 Differential pressure coefficient for the cold-gas jets flow.

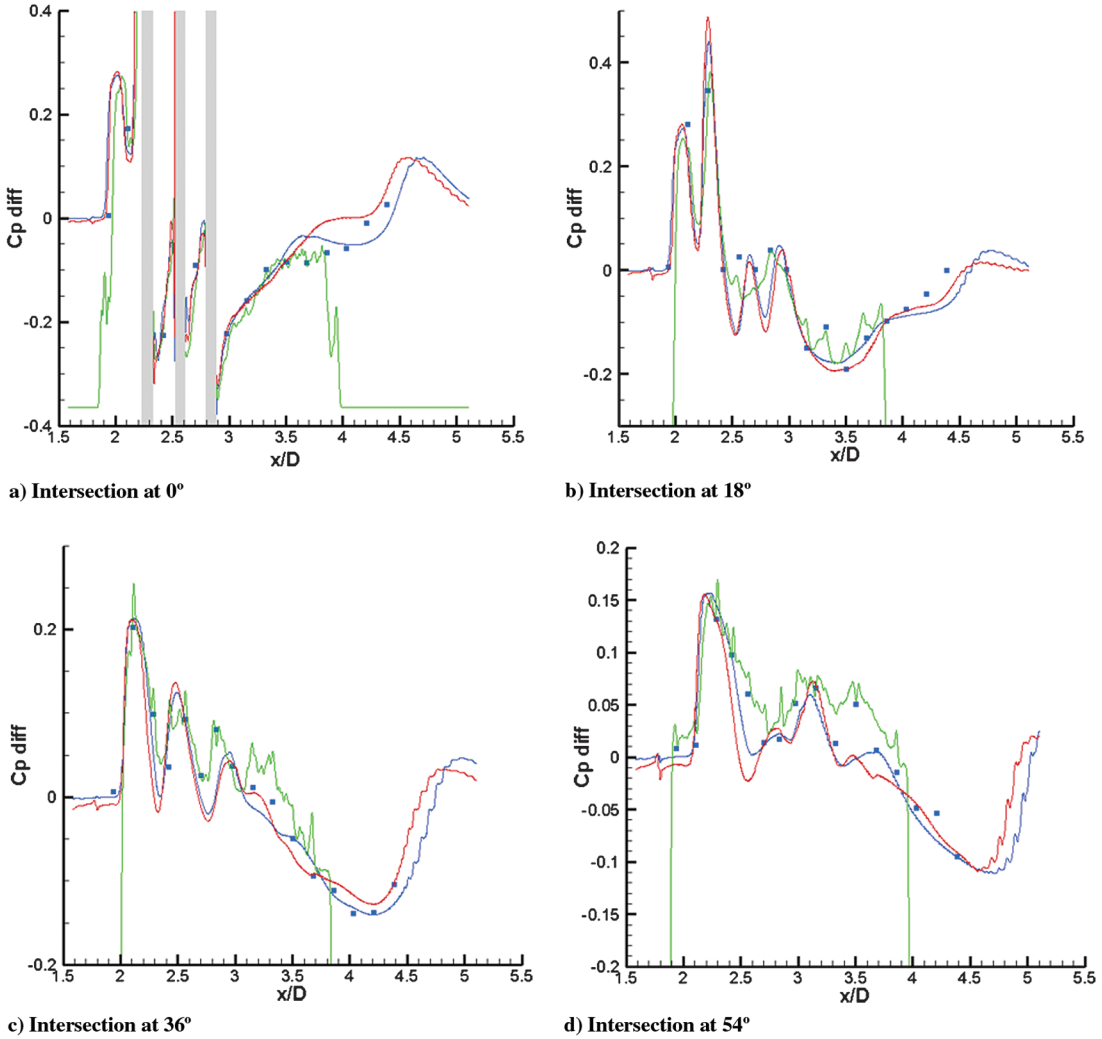


a) Intersection at 0° b) Intersection at 18°

c) Intersection at 36° d) Intersection at 54°

Fig. 22 Comparison of differential pressure coefficient between RANS computations on the fine grid and pressure measurements in the wind tunnel.

In a 120° angular sector on both sides of the symmetry plane, a good agreement can be observed between measurement in the wind tunnel and the RANS computation on the fine mesh of the cold-gas jets configuration. Beyond this region, it can be observed that the boundary layer at the bottom wall of the wind tunnel considerably influences the pressure on the body surface.

A more accurate comparison between all the configurations can be seen in Fig. 22. The mean value of the differential pressure coefficient measured in the wind tunnel and the numerical simulations have been traced on the same graphs, along the different intersections between the angular planes and the body (Fig. 19). It can be observed that numerical simulations of the real hot-gas jets and similar cold-gas jets configurations are reasonably close to each other as well as to pressure taps and PSP measurements. This result validates a posteriori the mesh refinements used for the computations.

The main differences occur in the symmetry plane, which is a boundary condition for the RANS computations on the fine meshes. In addition, the simulations have consisted of steady flow computations, whereas the flow under investigation is very unsteady. Unsteady RANS simulations, on a whole 3-D domain and taking into account the presence of other inactive thrusters, should improve the agreement with measurements in this plane.

The differences observed between the computations of real and similar flow can be partly explained by the fact that all the similarity numbers are not rigorously equal to 1. However, some other considerations have to be taken into account. The development of the boundary layer inside the nozzles is most likely different between real and similar thrusters, since they have completely different shapes. In addition, the kinematic viscosity in the external flow is also different, since different gases at different conditions are used. The method might be improved by accounting for these particular aspects, for instance, when defining the shape of cold-gases nozzles.

## V. Conclusions

A method has been suggested to substitute hot-gas lateral jets by cold-gas jets when investigating the interaction between lateral jet and supersonic flow. The main point has consisted of using the section ratio of thrusters to control a set of aerodynamic parameters, which are not commonly used for this kind of study, such as the wave celerity ratio. The method has been applied to a complex flow: a real rocket piloted by several interacting thrusters. Numerical and experimental investigations have revealed that a good approximation for the real lateral jets and crossflow interaction could be obtained using cold-gas jets instead.

This technique provides a modification of the manner that numerical methods and meshes are usually calibrated. Instead of trying to reproduce exactly the complex real flow in an experimental facility, a very similar and much easier-to-use configuration can be defined by this method. Grids and models can then be evaluated using this case and reliably implemented for the real flight computations.

This work has also brought a better understanding of the interaction between lateral jets and supersonic flow. The fact that similarity has been obtained between two completely different configurations means that aerodynamic interactions could be classified according to the suggested similarity numbers.

Such a classification could be interesting for semi-empirical aerodynamic models commonly used for trajectory computation. In these models, only the mechanical effect due to gas ejection is taken into account, whereas aerodynamic effects can strongly interfere with the surrounding lift surfaces. To model these effects, a virtual fin, reproducing the main aerodynamic effects of lateral jet, might be built. Parameters of the equivalent fin could be defined using the jet similarity parameters.

## Acknowledgments

We thank the German Ministry of Defense for supporting the current work under contract. We thank Jacques Haertig, now retired, and Friedrich Seiler for their major contribution to the development of experimental techniques at the French–German Research Institute of Saint-Louis.

## References

[1] Champigny, P., and Lacau, R. G., "Lateral Jet Control for Tactical Missiles," *Special Course on Missile Aerodynamics*, AGARD, Rept. R-804, Neuilly-sur-Seine, France, 6–10 June 1994, pp. 3.1–3.57.

[2] Cassel, L. A., "Applying Jet Interaction Technology," *Journal of Spacecraft and Rockets*, Vol. 40, No. 4, 2003, pp. 523–537. doi:10.2514/2.3992

[3] Beresh, S. J., Heineck, J. T., Walker, S. M., Schairer, E. T. and Yaste, D. M., "Planar Velocimetry of Jet/Fin Interaction on a Full-Scale Flight Vehicle Configuration," *AIAA Journal*, Vol. 45, No. 8, 2007, pp. 1827–1840. doi:10.2514/1.26485

[4] Beresh, S. J., Henfling, J. F., Erven, R. J., and Spillers, R. W., "Vortex Structure Produced by a Laterally Inclined Supersonic Jet in Transonic Crossflow," *Journal of Propulsion and Power*, Vol. 23, No. 2, 2007, pp. 353–363. doi:10.2514/1.25444

[5] Santiago, J. G., and Dutton, J. C., "Velocity Measurements of a Jet Injected into a Supersonic Crossflow," *Journal of Propulsion and Power*, Vol. 13, No. 2, 1997, pp. 264–273. doi:10.2514/2.5158

[6] Brandeis, J., and Gill, J., "Experimental Investigation of Super- and Hypersonic Jet Interaction on Missile Configurations," *Journal of Spacecraft and Rockets*, Vol. 35, No. 3, 1998, pp. 296–302. doi:10.2514/2.3354

[7] Graham, M. J., and Weinacht, P., "Numerical Investigation of Supersonic Jet Interaction for Axisymmetric Bodies," *Journal of Spacecraft and Rockets*, Vol. 37, No. 5, 2000, pp. 675–683. doi:10.2514/2.3617

[8] Graham, M. J., Weinacht, P., and Brandeis, J., "Numerical Investigation of Supersonic Jet Interaction for Finned Bodies," *Journal of Spacecraft and Rockets*, Vol. 39, No. 3, 2002, pp. 376–383. doi:10.2514/2.3836

[9] Sriram, A. T., and Mathew, J., "Numerical Simulation of Transverse Injection of Circular Jets into Turbulent Supersonic Streams," *Journal of Propulsion and Power*, Vol. 24, No. 1, 2008, pp. 45–54. doi:10.2514/1.26884

[10] Srivastava, B., "Computational Analysis and Validation for Lateral Jet Controlled Missiles," *Journal of Spacecraft and Rockets*, Vol. 34, No. 5, 1997, pp. 584–592. doi:10.2514/2.3272

[11] Min, B. Y., Lee, J. W., and Byun, Y. H., "Numerical Investigation of the Shock Interaction Effect on the Lateral Jet Controlled Missile," *Aerospace Science and Technology*, Vol. 10, No. 5, 2006, pp. 385–393. doi:10.1016/j.ast.2005.11.013

[12] Ebrahimi, H. B., "Numerical Investigation of Jet Interaction in a Supersonic Freestream," *Journal of Spacecraft and Rockets*, Vol. 45, No. 1, 2008, pp. 95–103. doi:10.2514/1.29847

[13] Champigny, P., and Leplat, M., "Aerodynamic Interference Induced by Lateral Jets on High Velocity Missiles," *Symposium on Innovative Missile Systems*, NATO RTO-AMP-AVT-135, Amsterdam, 15–18 May 2006.

[14] Lu, F. K., and Dickmann, D. A., "Topology of Supersonic Jet Interaction Flowfields at High Pressure Ratios," *13th International Symposium on Flow Visualization*, Nice, France, 1–4 July 2008.

[15] Bogdanoff, D. W., "Advanced Injection and Mixing Techniques for Scramjet Combustors," *Journal of Propulsion and Power*, Vol. 10, No. 2, 1994, pp. 183–190. doi:10.2514/3.23728

[16] Belanger, J., and Hornung, H. G., "Transverse Jet Mixing and Combustion Experiments in Hypervelocity Flows," *Journal of Propulsion and Power*, Vol. 12, No. 1, 1996, pp. 186–192. doi:10.2514/3.24009

[17] Gruber, M. R., Nejad, A. S., Chen, T. H., and Dutton, J. C., "Bow Shock/Jet Interaction in Compressible Transverse Injection Flowfields," *AIAA Journal*, Vol. 34, No. 10, 1996, pp. 2191–2193. doi:10.2514/3.13372

[18] Gnemmi, P., Schäfer, H. J., "Experimental and Numerical Investigations of a Transverse Jet Interaction on a Missile Body," *43rd AIAA Aerospace Sciences Meeting and Exhibit*, AIAA Paper 2005-0052, 2005.

[19] Gnemmi, P., Eichhorn, A., Leopold, F., Schaefer, H. J., Emunds, H., Esch, H., and Guelhan, A., "Experimental and Computational Study of

the Interaction between Lateral Jet and the Supersonic External Flow on a Generic Missile Body," *Symposium on Innovative Missile Systems*, NATO RTO-AMP-AVT-135, Amsterdam, 15–18 May 2006.

[20] Gnemmi, P., Adeli, R., and Longo, J., "Computational Comparisons of the Interaction of a Lateral Jet on a Supersonic Generic Missile," AIAA Atmospheric Flight Mechanics Conference, AIAA Paper 2008-6883, 2008.

[21] Havermann, M., Seiler, F., Weinand, K., Stern, D., and Zeiss, W., "Experimental and Numerical Analysis of Side-Jet Interference with a Mach-6 Cross Flow," *Symposium on Innovative Missile Systems*, NATO RTO-AMP-AVT-135, Amsterdam, 15–18 May 2006.

[22] ANSYS CFX, Software Package, Ver. 12.1, ANSYS Europe Ltd., Darmstadt, Germany, 2009.

[23] Menter, F. R., "Two-Equation Eddy-Viscosity Turbulence Models for Engineering Applications," *AIAA Journal*, Vol. 32, No. 8, 1994, pp. 1598–1605.
doi:10.2514/3.12149

[24] Sourgen, F., Gauthier, T., Leopold, F., Jagusinski, F., Sauerwein, B., Bastide, M., Seiler, F., Srulijes, J., and Meuer, R., "Bestimmung der Aerodynamischen Beiwerte für Komponenten einer Rakete," French–German Research Inst. of Saint-Louis, Rept. CR/RV 443/2009, Saint-Louis, France, 2009.

[25] Sourgen, F., Gauthier, T., Leopold, F., Jagusinski, F., Sauerwein, B., Bastide, M., Seiler, F., Srulijes, J., and Meuer, R., "Bestimmung der Aerodynamischen Beiwerte für Komponenten einer Rakete," French–German Research Inst. of Saint-Louis, Rept. RV 237/2010, Saint-Louis, France, 2010.

[26] Haertig, J., "Eléments sur le Traitement des Données Issues de Mesures en Général et de Vélocimétrie Laser en Particulier," *Ecole d'Automne de l'Association Francophone de Vélocimétrie Laser (AFVL)*, 2006.

[27] Liu, T., and Sullivan, J. P., *Pressure and Temperature Sensitive Paints*, Springer–Verlag, Berlin, 2005.

[28] Gregory, J. W., Asai, K., Kameda, M., Liu, T., and Sullivan, J. P., "A Review of Pressure-Sensitive Paint for High-Speed and Unsteady Aerodynamics," *Proceedings of the Institution of Mechanical Engineers, Part G (Journal of Aerospace Engineering)*, Vol. 222, No. 2, 2008, pp. 249–290.
doi:10.1243/09544100JAERO243

[29] Gauthier, T., Sourgen, F., Comet, M., Pichot, V., Spitzer, D., Piazzon, N., Leopold, F., and Martinez, B., "Nouvelles Possibilités des Peintures Sensibles à la Pression Nanostructurées (NanoPSP)," *13ième Congrès Français de Visualisation et de Traitement d'Images en Mécanique des Fluides (FLUVISU 13)*, Reims, France, 16–20 Nov. 2009.

[30] Gauthier, T., "Développement d'un Système PSP pour des Applications en Écoulement Supersonique," French–German Research Inst. of Saint-Louis, Rept. NI 904/2008, Saint-Louis, France, 2008.

R. Cummings
*Associate Editor*